Inorganic Chemistry

Article

pubs.acs.org/IC

$Sr_2Mn_3Sb_2O_2$ Type Oxyselenides: Structures, Magnetism, and Electronic Properties of $Sr_2AO_2M_2Se_2$ (*A*=Co, Mn; *M*=Cu, Ag)

Shifeng Jin,[†] Xiaolong Chen,*[,†] Jiangang Guo,[†] Ming Lei,[‡] Jingjing Lin,[†] Jianguo Xi,[‡] Wenjun Wang,[†] and Wanyan Wang[†]

[†]Research & Development Center for Functional Crystals, Beijing National Laboratory for Condensed Matter Physics, Institute of Physics, Chinese Academy of Sciences, Beijing 100190, China

[‡]School of Science, Beijing University of Posts and Telecommunications, Beijing 100876, China

Supporting Information

ABSTRACT: Four new oxyselenides with nominal formula $Sr_2AO_2M_2Se_2$ (*A*=Co, Mn; *M*=Cu, Ag) have been synthesized. They all crystallize in an *I*4/*mmm* space group and consist of alternating perovskite-like $(Sr_2AO_2)^{2+}$ blocks and antiflourie $(M_2Se_2)^{2-}$ layers, which are relatively rare layered oxyselenides reported so far that are isostructural to $Sr_2Mn_3Sb_2O_2$. From powder X-ray diffraction data, compounds $Sr_2CoO_2Cu_2Se_2$ and $Sr_2CoO_2Ag_2Se_2$ are found near stoichiometric, whereas $Sr_2MnO_2Cu_{2-\delta}Se_2$ and $Sr_2MnO_2Ag_{2-\delta}Se_2$ possess substantial copper or silver vacancies ($\delta \approx 0.5$), consistent with their oxysulfide analogues. X-ray photoelectron spectroscopy measurements indicate the readily oxidization of Mn^{2+} ions should be responsible for the occurrence of Cu/Ag vacancies. The rigid $(Sr_2AO_2)^{2+}$ blocks within these compounds constrain the basal lattice parameters in the *ab* plane and result in largely deformed tetrahedral sites for the large silver ions. Magnetic susceptibility measurements of $Sr_2CoO_2M_2Se_2$ (*M*=Cu, Ag) show complex antiferromagnetic transitions, while $Sr_2MnO_2M_{2-\delta}Se_2$ (*M*=Cu, Ag) show high-temperature Curie–Weiss behavior, followed by low-temperature antiferromagnetic transitions at 54 K and 67 K, respectively. Except for $Sr_2MnO_2Ag_{2-\delta}Se_2$, the other three compounds exhibit p-type semiconducting transport properties, with the measured resistivities several orders lower than their oxysulfide analogues. Hall measurement reveals high mobilities of $Sr_2CoO_2M_2Se_2$ (*M*=Cu, Ag) compounds at room temperature. The unusually small optical band gaps (~0.07 eV) of $Sr_2CoO_2Cu_2Se_2$, $Sr_2CoO_2Ag_2Se_2$, and $Sr_2MnO_2Cu_{2-\delta}Se_2$ are also reported.

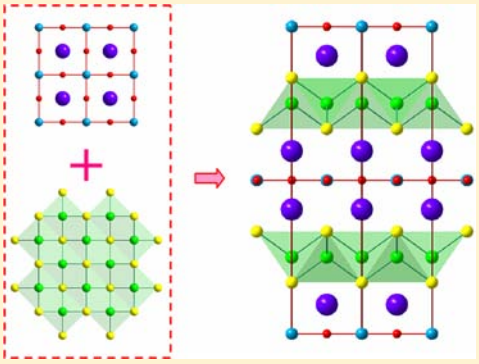

INTRODUCTION

In the past few years, oxychalcogenides have been a renewed interest with the discovery of compounds that exhibit novel electronic or magnetic properties[1−3] and intriguing structure features.[4−6] Due to the different sizes and coordination requirements of the oxide and the heavier chalcogenide anions, oxychalcogenides tend to adopt layered structures. For example, potential transparent p-type conductors *Ln*MOQ (*Ln* = rare-earth; *M* = Cu, Ag; *Q* = S, Se, Te) are a class of layered materials that consist of alternating $(Ln_2O_2)^{2+}$ fluorite layers and $(M_2Q_2)^{2-}$ antifluorite layers,[7,8] where the $(M_2Q_2)^{2-}$ layer is responsible for the interesting transport and optical properties.[9,10] Meanwhile, more complex oxychalcogenides can be found in which perovskite-type oxide layers are separated by antifluorite-type chalcogenide layers. For instance, the recently reported $Sr_{n+1}M'_nO_{3n-1}Cu_{2m}S_{m+1}$ series (*M*′ = transition metal) represent some examples of those compounds with various thicknesses of perovskite and antifluorite layers.[4] The great flexibility of those layers leads to a structural homologous series that dominate the known chemistry of oxychalcogenides.[11,12]

Oxychalcogenides in $Sr_2Mn_3Sb_2O_2$ structure type (space group *I*4/*mmm*)[13] are the most common members of the structural homologous series, where thicknesses of the oxide and chalcogenide layers are just one. The simple crystal structure of those compounds provides good opportunities to understand relevant systems. Currently, the most investigated such materials are corresponding oxysulfides, as in numerous examples of compounds $Sr_2AO_2Cu_2S_2$ (*A* = Co,[2] Mn,[14] Ni,[12] Cu,[12] and Zn[15,16]). In such cases, the transition-metal ions within oxide layers are in extremely square-planar environments, which make them ideal systems to investigate low dimensional magnetic coupling.[17] Mobile holes in $(Cu_2S_2)^{2-}$ layers also endow those compounds interesting transport properties. Moreover, the interactions of the two layers are found crucial to the compositions, structures, and physical properties of these compounds. For example, the oxidations of Mn in compound $Sr_2MnO_2Cu_{1.5}S_2$ were reported to have a direct impact on Cu site vacancies, and the Cu vacancies ordering in return determines the low-temperature superstructure and magnetic coupling of Mn ions.[11]

The layered oxychalcogenides of the $Sr_2Mn_3Sb_2O_2$ type have been found highly tolerant of ionic substitution in the perovskites oxide layers, which present rich opportunities for

Received: May 17, 2012
Published: September 11, 2012

   dx.doi.org/10.1021/ic301022g | *Inorg. Chem.* 2012, 51, 10185−10192

control of the magnetic properties. Besides the intensive studies on different transition-metal oxysulfides, a detailed investigation on the effect of alkali earth metal substitutions on the magnetism of $Sr_2CoO_2Cu_2S_2$ was reported recently.[17] However, although the $(M_2Q_2)^{2-}$ layer is considered to be the origin of the interesting transport and optical properties, structural engineering the antifluorite layer of the $Sr_2Mn_3Sb_2O_2$ type oxychalcogenides is far less exploited. The only reported oxyselenide of this type is $Ba_2ZnO_2Ag_2Se_2$,[18] which has a unique structure (space group *Cmca*) different from the above-mentioned oxysulfides (space group *I*4/*mmm*). The interaction between the thinnest perovskites layer and heavier chalcogenide layers (compared with CuS) and their effect on the compositions, structures, and electronic/magnetic properties of this class of oxychalcogenides are still ambiguous. It is clear that more systematic investigations on oxyselenides of this type are necessary to clarify these issues. In this work, we report the synthesis and structural characterization of four new layered manganese and cobalt oxyselenides, $Sr_2AO_2M_2Se_2$ (*A*=Co, Mn; *M*=Cu, Ag), wherein the anionic antifluorite layer is substantially altered by incorporating selenium and silver atoms. The magnetic, electronic transport and optical properties, structural variation tendency, and stability of these compounds are also investigated.

EXPERIMENTAL SECTION

Synthesis of $Sr_2AO_2M_2Se_2$ (*A*=Co, Mn; *M*=Cu, Ag). The quinary oxyselenides were obtained as bulk powders on the 1−2 g scale by grinding stoichiometric quantities of the reactants thoroughly in an agate pestle and mortar, pressing the mixtures into pellets at 10 MPa, and placing the pellets in dry alumina crucibles inside silica tubes that had been baked dry in a drybox for 2−3 h at 200 °C. The tubes were sealed under vacuum (10^{-4} Pa) and heated in an electrical resistance chamber furnace at temperatures of 900−1000 °C for 24−72 h, followed by cooling at the natural rate of the furnace. Starting materials were as follows: Cu powder (Sinopharm, 99.99%), Ag powder (Alfa Aesar, 99.95%), Mn powder (Sinopharm, 99.99%), and Co powder (Sinopharm, 99.99%). SrO was prepared by decomposing $Sr(NO_3)_2$ (Sinopharm, 99.5%) under air atmosphere at 800 °C for 24 h with a final firing of 3 h at 1100 °C. Due to the air sensitivity of many of the reagents and the products, manipulations of the solids prior to synthesis were always performed in a Mikrouna (China) Co., Ltd. argon-filled glovebox with an O_2 and H_2O content of less than 1 ppm.

For instance, phase pure samples of $Sr_2CoO_2Cu_2Se_2$ and $Sr_2CoO_2Ag_2Se_2$ were obtained by reacting the stoichiometric reactants at 900 °C for 48 h. Both of the compounds thus obtained are shiny dark black pellets. The chemical equation can be written as

$$2SrO + Co + 2M\ (\text{Cu or Ag}) + 2Se \rightarrow Sr_2CoO_2M_2Se_2$$

Meanwhile, the sample of $Sr_2MnO_2Cu_2Se_2$ was obtained by lifting the reaction temperature up to 1000 °C and kept there for 24 h. For this compound, the stoichiometric reactants always lead to the appearance of a considerable amount of copper metal on the surface of the pellets, indicating there are considerable copper deficiencies in this oxyselenide. Subsequently, phase-pure (by PXRD) bulk material for structure refinement and property measurements was made on the 2 g scale by using the following chemical equation

$$2SrO + Mn + 1.5M\ (\text{Cu or Ag}) + 2Se \rightarrow Sr_2MnO_2M_{1.5}Se_2$$

For compound $Sr_2MnO_2Ag_{1.5}Se_2$, phase pure samples cannot be obtained via traditional high-temperature solid-state reaction. Both of the reacting temperature and reactant composition have been tuned to increase the yield of the quinary phase, and the result reported here that gives the best yield is obtained by following the above chemical equation at 900 °C for 72 h.

Crystal Structure Determinations. X-ray powder diffraction patterns were used for the purpose of phase characterization and Rietveld refinement. The X-ray powder diffraction patterns were recorded at room temperature on a Panalytical diffractometer (X'Pert PRO MRD) with Cu Kα radiation (40 kV, 40 mA) and a graphite monochromator in a reflection mode (2θ = 5−135°, step = 0.017°, scan speed = 5s/step). Well grounded fine powder samples on glass slides were used to collect the diffraction pattern.

Phase characterizations were realized from powder patterns using the PDF2-2010 database. Indexing of the compounds was realized from the phase pure powder patterns using the DICVOL91 program.[19] For compound $Sr_2MnO_2Ag_2Se_2$ the indexing was performed by manually excluding impurity peaks. Rietveld refinement was performed using the FULLPROF program.[20]

X-ray Photoelectron Spectroscopy (XPS). The XPS data were taken on an AXIS-Ultra instrument from Kratos using monochromatic Al K_α radiation (225 W, 15 mA, 15 kV) and low-energy electron flooding for charge compensation. To compensate for surface charges effects, binding energies were calibrated using the C1s hydrocarbon peak at 284.80 eV. The XPS data were converted into the VAMAS file format and imported into the CasaXPS software package for manipulation and curve-fitting.

Magnetic Susceptibility Measurements. Measurements were carried out using Quantum Design PPMS magnetometers in the temperature range 10−300 K and at magnetic fields of 0.1 T. Approximately 20−40 mg of material was weighed accurately into a gelatin capsule. Measurements of the susceptibility were made on warming in measuring fields of 0.1 T after cooling in zero field (zero-field-cooled: ZFC) and then again on warming after cooling in the measuring field (field-cooled: FC).

Transport Measurements. The electrical conductivity measurements of the title compounds were obtained using the four probe technique on a Quantum Design PPMS DC module. Electrical contacts consisted of fine platinum wire attached to the sintered pellet with silver paste. To improve contact performance, the samples were placed within the glovebox for at least 24 h to allow the silver paste to cure completely. Excitation currents were kept as low as possible, typically below 1 mA, to minimize nonohmnic voltage response and thermoelectric effects at the contact-sample interface. Measurements of the sample cross-sectional area and voltage probe separation were made with a microcalliper.

Hall Measurements. Measurements were performed on an Accent HL5500 Hall System in measuring field of 0.516 T. The sintered samples in square pellet form were measured using the Van der Pauw method at room temperature.

UV−vis-IR Diffuse Reflectance Spectroscopy. The UV−vis-IR optical reflectance data over the spectral range 240−2600 nm were collected on a Tu-1901 reflection spectrometer at room temperature. $BaSO_4$ was used as a reference material. Reflectance spectra were converted to absorbance using the Kubelka−Munk function.

Infrared Spectroscopy Measurement. Infrared spectra were recorded on a Perkin-Elmer 983 infrared spectrophotometer in the 400 to 4000 cm^{-1} wavenumber range using the KBr pellets. To prevent H_2O contaminations, the title compounds (5‰ by mass) and KBr were mixed and pressed within an argon-filled glovebox.

RESULTS AND DISCUSSION

Crystal Structures and Compositions. As shown in Figure 1, laboratory PXRD measurements of the $Sr_2CoO_2Cu_2Se_2$ sample revealed no impurity phases. Refinement against the room-temperature data on this sample produced the results summarized in Tables 1and 2 and the crystal structure shown in Figure 2. The compound was found crystallized in structure type $Sr_2Mn_3Sb_2O_2$, with space group *I*4/*mmm*. The structure contains infinite CoO_2 sheets with Co^{2+} ions in square planar coordination by four oxide ions; Cu^+ ions are coordinated tetrahedrally by selenium, forming antifluorite type Cu_2Se_2 layers, and the two anionic layers are

dx.doi.org/10.1021/ic301022g | *Inorg. Chem.* 2012, 51, 10185−10192

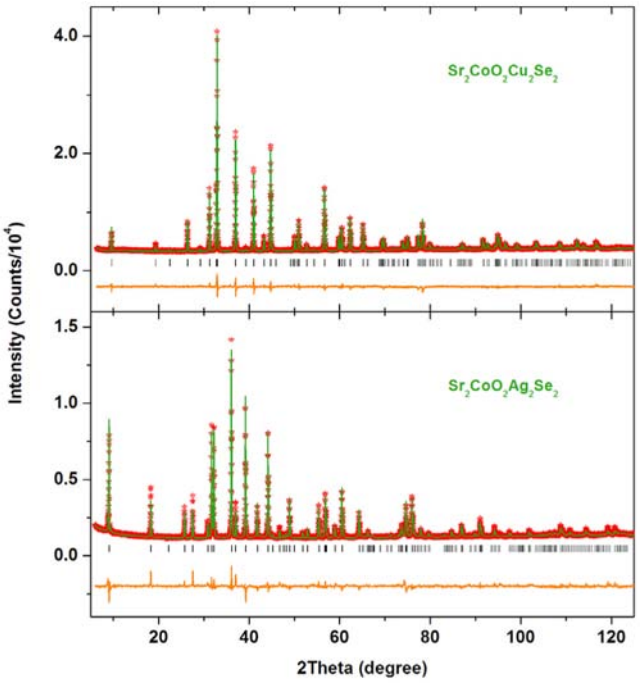

Figure 1. Result of Rietveld refinement against powder XRD diffraction data for samples of $Sr_2CoO_2Cu_2Se_2$ (upper) and $Sr_2CoO_2Ag_2Se_2$ (lower). The data (red points), fit (green line), and difference (yellow lower line) are shown with tick marks indicating reflection positions.

Table 2. Fractional Atomic Coordinates and Equivalent Isotropic Displacement Parameters for $Sr_2CoO_2Cu_2Se_2$(I), $Sr_2CoO_2Ag_2Se_2$(II), $Sr_2MnO_2Cu_{1.5}Se_2$(III), and $Sr_2MnO_2Ag_{1.5}Se_2$(IV)[a]

	atom	*x*	*y*	*z*	U_{iso} (Å^2)	occ
I	Sr	0	0	0.4119(1)	0.0136(4)	1.0
	Co	0	0	0	0.0231(10)	1.0
	O	0	1/2	0	0.0232(1)	1.0
	Cu	0	1/2	1/4	0.0258(7)	0.995(3)
	Se	0	0	0.1679(1)	0.0176(5)	1.0
II	Sr	0	0	0.4166(1)	0.0185(8)	1.0
	Co	0	0	0	0.016(2)	1.0
	O	0	1/2	0	0.0133(1)	1.0
	Ag	0	1/2	1/4	0.0278(7)	0.982(3)
	Se	0	0	0.1545(2)	0.0218(10)	1.0
	Sr	0	0	0.4049(1)	0.0175(6)	1.0
	Mn	0	0	0	0.0158(12)	1.0
III	O	0	1/2	0	0.0225(8)	1.0
	Cu	0	1/2	1/4	0.0236(11)	0.758(4)
	Se	0	0	0.1670(1)	0.0193(7)	1.0
	Sr	0	0	0.4105(1)	0.0221(5)	1.0
	Mn	0	0	0	0.0262(11)	1.0
IV	O	0	1/2	0	0.028(3)	1.0
	Ag	0	1/2	1/4	0.0394(7)	0.720(2)
	Se	0	0	0.1548(1)	0.0247(5)	1.0

[a]The chemical composition is based on the site occupancies obtained from Rietveld refinements.

separated by Sr ions. The as prepared sample was very close to stoichiometric in copper, with a refined composition of $Sr_2CoO_2Cu_{1.990(6)}Se_2$. In comparision with $Sr_2CoO_2Cu_2S_2$, the unit cell enlargement is moderate and more obvious for lattice parameters *c* (from 17.7156(1) to 18.3571(2) Å) than for parameter *a* (from 3.9913(1) to 4.0488(1) Å), giving a difference in cell volume of 6.21%. Table 3 lists the important bond lengths and angles obtained from refinement, where the Cu−Se bond length of 2.5235(7) for $Sr_2CoO_2Cu_{1.990(6)}Se_2$ is comparable to the values of 2.52(1) and 2.51(1) Å in the oxyselenide LaOCuSe and BiOCuSe, respectively.[10] Meanwhile, the Co−Se bond length 3.0827(11) Å is much longer than the regular Co−Se bond lengths (e.g., 2.474(2) Å in hexagonal CoSe), indicating the Co atoms have a rather weak bonding to their apical Se atoms. The flexible $(Cu_2Se_2)^{2-}$ layers respond to the constraint from the more rigid $(Sr_2CoO_2)^{2+}$ layers by a moderate squashing of the $CuSe_4$ tetrahedra along the *a* and *b* axis. As shown in Table 3, two bond angles of Se−Cu−Se slightly deviated from 109°28′ into 110.88(1)° and 106.69(3)° respectively.

Table 1. Results of Powder X-ray Diffraction and Rietveld Refinements for $Sr_2CoO_2Cu_2Se_2$, $Sr_2CoO_2Ag_2Se_2$, $Sr_2MnO_2Cu_{1.5}Se_2$, and $Sr_2MnO_2Ag_{1.5}Se_2$ at Room Temperature[a]

formula	$Sr_2CoO_2Cu_2Se_2$	$Sr_2CoO_2Ag_2Se_2$	$Sr_2MnO_2Cu_{1.5}Se_2$	$Sr_2MnO_2Ag_{1.5}Se_2$
molecular weight	551.184	639.828	547.189	581.899
lattice	tetragonal	tetragonal	tetragonal	tetragonal
space group	*I*4/*mmm*	*I*4/*mmm*	*I*4/*mmm*	*I*4/*mmm*
a (Å)	4.0488(1)	4.0980(1)	4.0689(1)	4.0882(1)
c (Å)	18.3571(2)	19.4316(2)	17.8760(2)	19.1179(2)
V (Å^3)	300.918(3)	326.327(5)	295.960(6)	319.525(5)
Z	2	2	2	2
T/K	298(2)	298(2)	298(2)	298(2)
D_x (g cm^{-3})	5.79	5.98	5.45	5.47
radiation type	Cu *Kα*	Cu *Kα*	Cu *Kα*	Cu *Kα*
wavelength (Å)	1.5418	1.5418	1.5418	1.5418
collection range (°2*θ*)	5−135	5−125	5−135	5−135
step size (°2*θ*)	0.017	0.017	0.017	0.017
R_p (%)	2.08	3.36	4.14	3.57
R_{wp} (%)	2.77	4.67	5.59	4.57
S	1.73	1.78	1.70	1.70

[a]The chemical composition is based on the site occupancies obtained from Rietveld refinements. $R_p = \sum|y_{io}-y_{ic}|/\sum|y_{io}|$, $R_{wp}=[\sum w_i(y_{io}-y_{ic})^2/\sum w_i y_{io}^2]^{1/2}$, $S = \sum[w_i(y_{io}-y_{ic})^2/(N-P_1-P_2)\ ]^{1/2}$.

dx.doi.org/10.1021/ic301022g | *Inorg. Chem.* 2012, 51, 10185−10192

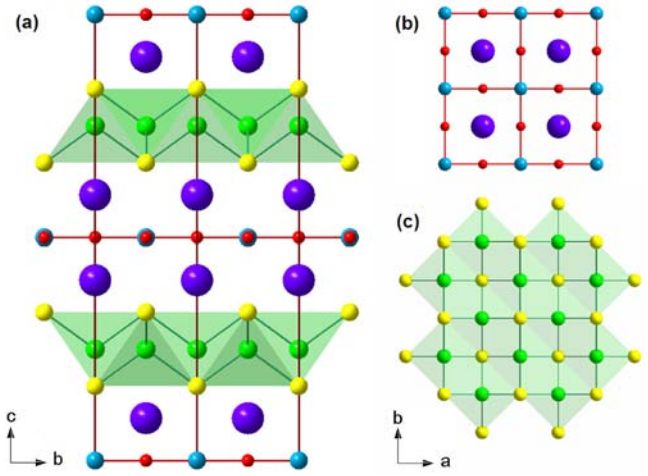

Figure 2. (a) The room-temperature structures of $Sr_2AO_2M_2Se_2$ (A=Co, Mn; M=Cu, Ag), structure details of Sr_2AO_2 layers (b) and M_2Se_2 layer (c) are also given. (Color key: purple: Sr; light blue: Co; red: O; green: Cu; yellow: Se).

Table 3. Typical Bond Lengths (Å) and Bond Angles (deg) of $Sr_2CoO_2Cu_2Se_2$(I), $Sr_2CoO_2Ag_2Se_2$(II), $Sr_2MnO_2Cu_{1.5}Se_2$(III), and $Sr_2MnO_2Ag_{1.5}Se_2$(IV)

bond/angle	*I*	*II*	*III*	*IV*
(Cu/Ag)−Se (Å)	2.5235(7) × 4	2.7647(14) × 4	2.5177(9) × 4	2.7376(9) × 4
(Co/Mn)−O (Å)	2.0244(1) × 4	2.0490(1) × 4	2.0345(1) × 4	2.0441(1) × 4
Sr−O (Å)	2.5910(7) × 4	2.6129(12) × 4	2.6508(9) × 4	2.6654(7) × 4
(Co/Mn)−Se (Å)	3.0827(11) × 2	3.002(2) × 2	2.9858(16) × 2	2.9585(13) × 2
Se−(Cu/Ag)−Se (deg)	110.88(1) × 4	116.79(3) × 4	110.31(2) × 4	116.26(2) × 4
	106.69(3) × 2	95.66(5) × 2	107.81(4) × 2	96.61(3) × 2

Successful synthesis of $Sr_2CoO_2Cu_2Se_2$ encouraged us to expand the CoO_2 planes further by substituting larger coinage-metals for Cu. A sample of composition $Sr_2CoO_2Ag_2Se_2$ was successfully prepared in a similar routine as described for $Sr_2CoO_2Cu_2Se_2$. The as-synthesized sample was dark shining black, without noticeable impurities in the laboratory PXRD measurements. Subsequent refinement against the room-temperature data (Figure 1) reveals an analogue *I*4/*mmm* structure (Figure 2), with a refined composition of $Sr_2CoO_2Ag_{1.964(6)}Se_2$. The analysis suggests that, similar to the case of $Sr_2CoO_2Cu_2Se_2$ and $Sr_2CoO_2Cu_2S_2$, there is a small (0.5−2%) intrinsic coinage-metal deficiency in this system. Lattice parameters of this compound are further expanded up to a = 4.0980(1) Å and c = 19.4316(2) Å. It is worth noticing that the significantly enlarged unit cell of $Sr_2CoO_2Ag_2Se_2$ corresponds to the largest CoO_2 square plane ever reported. As a comparison, lattice parameter a of provoskite $SrCoO_3$ is 3.835(2) Å, while the recently reported $Ba_2CoO_2Cu_2Se_2$ is 4.0711(1) Å.[17] Expansion of the lattice parameter a is limited by the maximum Co−O bond length that can be maintained within the CoO_2 plane. On the other hand, the c parameter can accommodate much greater expansion. Silver atom substitution leads to a 5.85% increase in c, which is more than 4.7 times greater than the 1.22% increase in a. From the two bond angles of Se−Ag−Se shown in Table 3 (116.79(3)° and 95.66(5)°), it is found that the larger $(Ag_2Se_2)^{2-}$ layers were seriously deformed.

Unlike cobalt oxychalcogenides, where stoichiometry can be obtained after great care, most of the manganese oxysulfides inevitably contain considerable Cu vacancies. Our attempts to produce stoichiometric $Sr_2MnO_2Cu_2Se_2$ also revealed considerable copper metals precipitated on the surface of the sample, similar to the result of $Sr_2MnO_2Cu_{1.5}S_2$. Subsequently, phase-pure (by PXRD) bulk material was made with nominal composition $Sr_2MnO_2Cu_{1.5}Se_2$. Refinement against the room temperature data (Figure 3) using the *I*4/*mmm* model

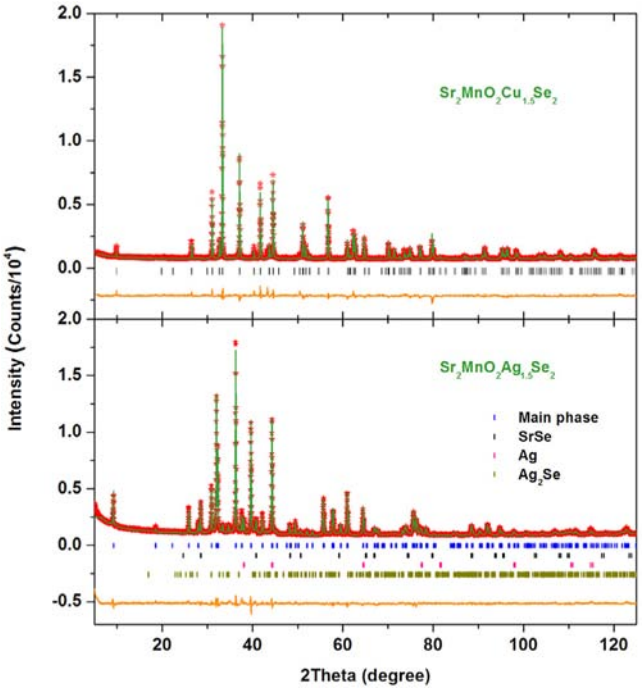

Figure 3. Result of Rietveld refinement against powder XRD diffraction data for samples of $Sr_2MnO_2Cu_{1.5}Se_2$ (upper) and $Sr_2MnO_2Ag_{1.5}Se_2$ (lower). The data (red points), fit (green line), and difference (yellow lower line) are shown with tick marks indicating reflection positions of the main and some impurity phases. The chemical composition is based on the site occupancies obtained from Rietveld refinements.

produced a refined composition of $Sr_2MnO_2Cu_{1.516(8)}Se_2$, with lattice parameters a = 4.0689(1) Å and c = 17.8760(2) Å. We noticed that Clarke et al.[11] mentioned an unpublished result on this compound stating that it contains analogue copper deficiencies in comparision with $Sr_2MnO_2Cu_{1.5}S_2$, which is consistent with our refinement results.

On the other hand, the compound with nominal formula $Sr_2MnO_2Ag_{1.5}Se_2$ cannot be obtained in a pure form with the high-temperature synthesis route, the X-ray analyses of the product revealed a mixture of the target compound with minor SrSe, Ag, and Ag_2Se impurities. PXRD Rietveld refinement was attempted for this multiphase sample, as shown in Figure 3.Using the *I*4/*mmm* model, the refinement converged readily to satisfying reliability factors (see Table 1). Quantitative phase analysis revealed 73.41% by mole the target phase, 13.91% SrSe, 5.81% Ag_2Se, and 6.87% Ag impurity phases, respectively. There should also be some ill crystallized manganese oxide impurities by taking account of the starting composition. The target compound was found also inherent with considerable Ag

dx.doi.org/10.1021/ic301022g | *Inorg. Chem.* 2012, 51, 10185−10192

vacancies, with a refined composition of $Sr_2MnO_2Ag_{1.440(4)}Se_2$. The analysis suggests that, similar to the case of $Sr_2MnO_2Cu_{1.5}Se_2$, there is about 25% silver deficiency in the system based on the refinements. The nominal compositions and synthesis temperatures were subsequently tuned but failed to improve the yield. Beside $Sr_2MnO_2Ag_{1.5}Se_2$, there have been several oxychalcogenides that cannot be obtained in a pure form, such as $Sr_2NiO_2Cu_2S_2$, $Sr_2Cu_3O_2S_2$, and $Sr_3Fe_2Ag_2Se_2O_5$.[12,21] The impurity within $Sr_2NiO_2Cu_2S_2$ and $Sr_2Cu_3O_2S_2$ is attributed to readily reduction of Ni^{2+} and Cu^{2+} transition metals at high temperature. However, the large impurities appear in $Sr_3Fe_2Ag_2Se_2O_5$ and $Sr_2MnO_2Ag_{1.5}Se_2$ cannot be ascribed to a similar reason, since both $Sr_3Fe_2Cu_2Se_2O_5$ and $Sr_2MnO_2Cu_{1.5}Se_2$ can be obtained phase pure. Instead, the significantly enlarged silver selenium layers and the resulting stress within the transition metal−oxygen layers might be responsible to the instability of the above-mentioned oxychalcogenides.

Mn Valence State. With the presence of less electronegative chalcogenide atoms, transition metals in the oxychalcogenides tend to exhibit lower oxidation states than in perovskite-type oxides. For oxyselenides with the general formula $Sr_2AO_2M_2Se_2$, both of the A^{2+} and M^+ metals are in their low oxidation states. However, the appearance of considerable Cu/Ag vacancies in the manganese compounds requires a higher oxidation state for the Mn or Cu/Ag ions. One natural hypothesis raised during the investigation of $Sr_4Mn_2O_4Cu_5S_5$ is that the manganese oxidation state is 2+, which would require holes in the copper chalcogenide layers, as in the metals KCu_4S_3, $TlCu_{2n}S_{n+1}$, and $Bi_2YO_4Cu_2Se_2$.[22] However, a recent investigation on magnetism of $Sr_2MnO_2Cu_{1.5}S_2$ indicated that the Mn ions are more likely in high spin 2.5+ state. To provide more direct evidence to the valence state of Mn and Cu ions, the XPS Mn2p and Cu2p spectra were subsequently obtained for the as synthesized $Sr_2MnO_2Cu_{1.5}Se_2$. As shown in Figure 4a, the $Mn2p_{3/2}$ photopeak binding energy maxima for this compound is 641.41 eV, which lies in between the binding energies of Mn^{2+} and Mn^{3+} ions in MnO (640.4 eV) and Mn_2O_3 (641.9 eV), and corresponds well to the $Mn2p_{3/2}$ binding energy of Mn_3O_4 (641.4 eV).[23] The result indicates that the Mn ions within $Sr_2MnO_2Cu_{1.5}Se_2$ adopt a mixed valence 2.5+ state. Meanwhile, the profiles of $Cu2p_{3/2}$ and $Cu2p_{1/2}$ signals show no obvious multiplet peaks and satellite peaks that are inherent with Cu^{2+} ions, indicating the disordered Cu ions predominately adopt the monovalence state. The results confirm the occurrence of Cu vacancies is due to the readily oxidization of Mn^{2+} ions.

Structural Trends. When Smura et al.[17] substitute the Ba atoms for Sr atoms in a series of solid solution $(Sr_{1-x}Ba_x)_2CoO_2Cu_2S_2$, they find the soft $(Cu_2S_2)^{2-}$ layers are readily squashed along the *c* axis. Meanwhile, the unit cell enlargement along the *a* axis is hindered by strong Co−O bonds, resulting in more obvious expansion of lattice parameters *c*. In the current work, the metal chalcogenide layer is substantially expanded upon selenium and silver substitutions. Using the metal chalcogenide bond lengths found in $Sr_2CoO_2Cu_2S_2$ and two Co compounds reported herein, the lattice parameter *a* of the compounds containing undeformed Cu−S, Cu−Se, and Ag−Se layers should be 3.9772(5) Å, 4.122(2) Å, and 4.515(3) Å, respectively. Meanwhile, in cases where Co is coordinated tetrahedrally by four oxide ions in the presence of large electropositive ions, mean bond lengths rarely exceed 2 Å (the Co−O distance is

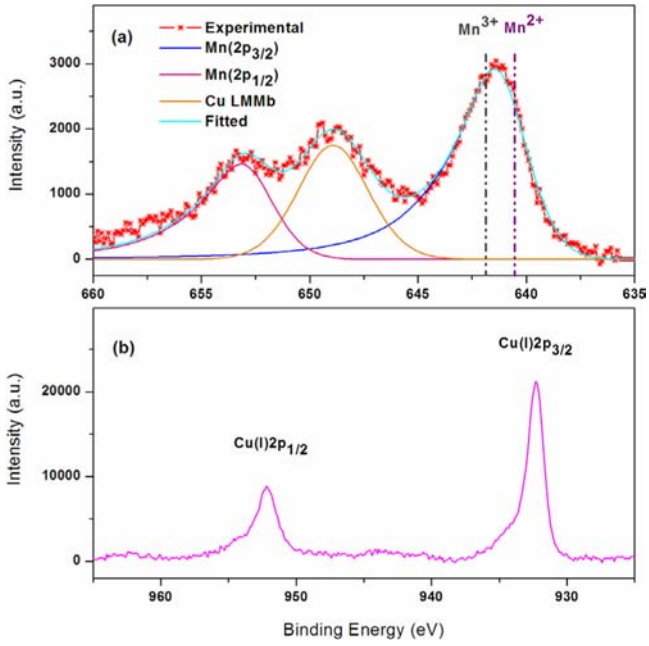

Figure 4. (a) XPS Mn 2p signals of compound $Sr_2MnO_2Cu_{1.5}Se_2$ after background subtraction. The profile is fit by three peaks, corresponding to Mn $2p_{3/2}$, Cu_{LMMb}, and Mn $2p_{1/2}$, respectively. The two dashed lines correspond to the binding energies of Mn^{2+} and Mn^{3+} ions in MnO and Mn_2O_3. (b) XPS Cu $2p_{3/2}$ and Cu $2p_{1/2}$ signals after background subtraction.

equal to half of the parameter *a*). The different requirement for cell parameters from the chalcogenide and oxide layers is thus significantly enhanced by selenium and especially silver substitutions.

As a key structure feature, it is found that the substituted metal chalcogenide layers are seriously deformed with element substitutions, while the rigid metal oxide layers only expand slightly. As shown in Table 3, the varying bond angles of Se−Cu−Se and Se−Ag−Se indicate the large metal chalcogenide layers are readily squashed within the *ab* plane, so that the deformed layers basically expand along the *c* direction (see Table 1). Consequently, the lattice parameter for the substituted stoichiometric Co compounds make a 3.62% and 9.69% increase in parameter *c*, which is about 3 times higher than the expansion of parameter *a* (1.44% and 2.67% respectively). The flexibility of the metal chalcogenide layer is essential in enabling selenium and silver substitution to occur in this structure type. The structural trends of metal chalcogenide layer substitution are found quite consistent for the Co and Mn compounds; only the mean metal-chalcogenide bond length of the Mn compounds are systematically shorter than the Co compounds, which is possibly due to the presence of substantial coin-metal vacancies. It is worth noticing that apart from deforming the metal chalcogenide layer, the early reported $Ba_2ZnO_2Ag_2Se_2$ accommodates to the substitutions by altering and expanding the metal oxide layers, which results in a rare structure type containing discrete $(ZnO_2)^{2-}$ linear anionic units.[18]

Magnetic Properties. As shown in Figure 5, the magnetic susceptibility data show broad maxima for both compounds $Sr_2CoO_2Cu_2Se_2$ and $Sr_2CoO_2Ag_2Se_2$, consistent with their sulfide analogues. Particularly, magnetic susceptibility of $Sr_2CoO_2Cu_2Se_2$ and $Sr_2CoO_2Ag_2Se_2$ shows a broad maximum at about 250 and 210 K, respectively, suggestive of low-

dx.doi.org/10.1021/ic301022g | Inorg. Chem. 2012, 51, 10185−10192

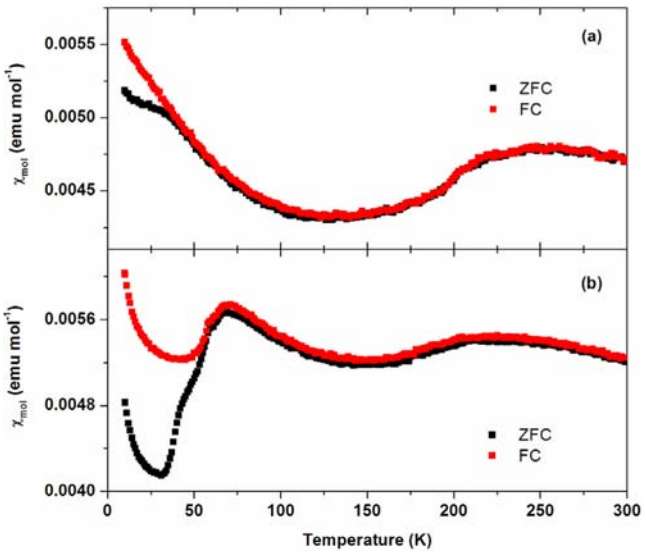

Figure 5. Zero-field and field-cooled magnetic susceptibilities for $Sr_2CoO_2Cu_2Se_2$ (a) and $Sr_2CoO_2Ag_2Se_2$ (b) measured at 0.1 T.

dimensional antiferromagnetic ordering of the cobalt sublattice. $Sr_2CoO_2Ag_2Se_2$ shows a second maximum at a lower temperature (70 K), which is similar to La_2CoO_4 and $Ba_2CoO_2Cu_2S_2$ that have successive antiferromagnetic transitions. In addition to the broad transitions at higher temperatures, a crossover, possibly antiferromagnetic to spin glass transition, take place at about 37 K ($Sr_2CoO_2Cu_2Se_2$) and 60 K ($Sr_2CoO_2Ag_2Se_2$) respectively. The difference observed between FC and ZFC susceptibilities beginning at these temperatures suggests spin-glass freezing of magnetic clusters. A Curie-like term in the susceptibility of $Sr_2CoO_2Ag_2Se_2$ at low temperatures presumably arises from paramagnetic impurities.

Figure 6 shows the magnetic susceptibilities measured as functions of temperature on the samples of $Sr_2MnO_2Cu_{1.5}Se_2$ and $Sr_2MnO_2Ag_{1.5}Se_2$ used for PXRD investigations. Magnetic susceptibility measurements show sharp peaks for the two compounds under a measurement field of 0.1 T, suggesting antiferromagnetic ordering of the sole magnetic cation Mn in compounds $Sr_2MnO_2Cu_{1.5}Se_2$ and $Sr_2MnO_2Ag_{1.5}Se_2$. The consistency of zero-field-cooled and field-cooled data precludes the possibility of spin-glass freezing in this system. The observation for these two Mn compounds is consistent with previous observations for $Sr_2MnO_2Cu_{1.5}S_2$, with the exception that the antiferromagnetic transition temperature is much elevated with element substitutions. For instance, the antiferromagnetic ordering of $Sr_2MnO_2Cu_{1.5}Se_2$ and $Sr_2MnO_2Ag_{1.5}Se_2$ occurs at 54 K and 67 K respectively, which is much higher than the transition temperature reported for $Sr_2MnO_2Cu_{1.5}S_2$ (29.5 K). The antiferromagnetic transition temperature seems increase monotonically with the expansion of the MnO_2 layers within the *ab* plane. In Figure 6, we also give the temperature dependence of the inverse susceptibility ($1/\chi$). A linear temperature dependence of $1/\chi$ is found from 300 K to about 150 K. The magnetic susceptibility is, hence, analyzed by the Curie–Weiss law

$$\chi = \frac{C}{T - \theta}$$

where C and θ are the Curie constant and the Weiss temperature, respectively. The Curie constant for samples of

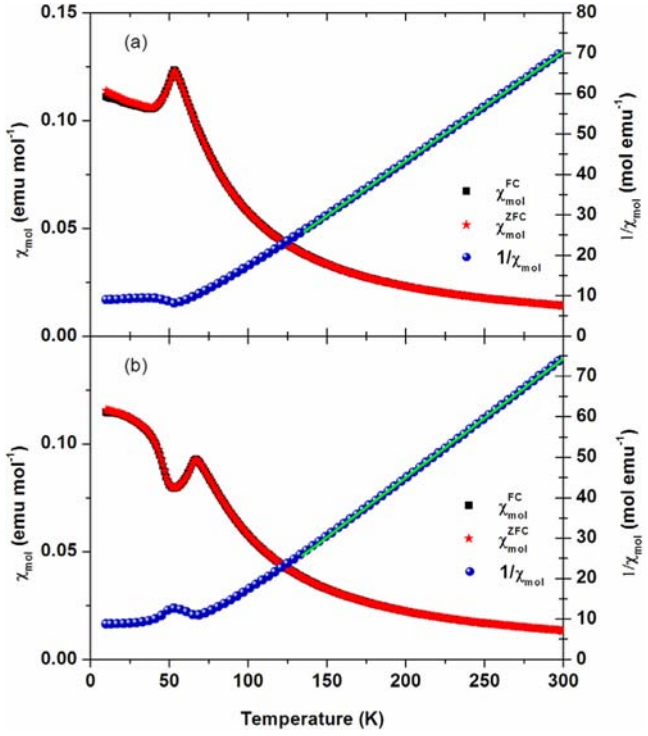

Figure 6. Zero-field and field-cooled magnetic susceptibilities for $Sr_2MnO_2Cu_{1.5}Se_2$ (a) and $Sr_2MnO_2Ag_{1.5}Se_2$ (b) measured at 0.1 T. Liner fit to the Curie–Weiss law is shown as green solid lines.

$Sr_2MnO_2Cu_{1.5}Se_2$ is fairly consistent with that reported for $Sr_2MnO_2Cu_{1.5}S_2$. The effective magnetic moment u_{eff} for $Sr_2MnO_2Cu_{1.5}Se_2$ is determined to be 5.46(1) u_B, which is significantly lower than the spin-only u_{eff} of 5.92 u_B expected for the high spin d^5 configuration of Mn^{2+}, but agrees well with the value of 5.43 u_B expected for a mean oxidation state of $Mn^{2.5+}$. Comparatively, an effective magnetic moment (u_{eff}) of 5.3–5.4 u_B per manganese ion was reported for $Sr_2MnO_2Cu_{1.5}S_2$. Data fitting for the $Sr_2MnO_2Ag_{1.5}Se_2$ yield a higher effective moment (u_{eff} = 5.82(1) u_B), the value might well be overestimated due to some ill crystallized manganese oxide impurities. The positive Weiss temperatures for $Sr_2MnO_2Cu_{1.5}Se_2$ (+39.9 K) and $Sr_2MnO_2Ag_{1.5}Se_2$ (+46.8 K) revealed the dominant exchange interactions in the temperature range 150–300 K are ferromagnetic.

Transport Properties. The oxide and chalcogenide layers in these compounds may be considered quite electronically distinct. Previous works on some analogue oxysulfides and simpler *Ln*OCu*Ch* (*Ln* = lanthanide, *Ch* = S, Se, Te) give evidence that those compounds are an intergrowth of charge-carrying chalcogenide layers and insulating oxide layers.[11] While the charge-carrying chalcogenide layers of the title compounds have been subsequently altered and deformed by element substitution, their electric transport properties should be more directly affected. As shown in Figure 7, measurement of the electrical resistivities of $Sr_2CoO_2Cu_2Se_2$, $Sr_2CoO_2Ag_2Se_2$, and $Sr_2MnO_2Cu_{1.5}Se_2$ showed that all three compounds are semiconducting. The resistivities increase rapidly on cooling from room temperature values of 0.0418(1) Ωcm for $Sr_2CoO_2Cu_2Se_2$, 0.115(1) Ωcm for $Sr_2CoO_2Ag_2Se_2$, and 0.079(1) Ωcm for $Sr_2MnO_2Cu_2Se_2$. The resistivity values are systematically several orders lower than that of the analogue oxysulfides $Sr_2CoO_2Cu_2S_2$ (~4 Ωcm at 300 K) and

dx.doi.org/10.1021/ic301022g | *Inorg. Chem.* 2012, 51, 10185–10192

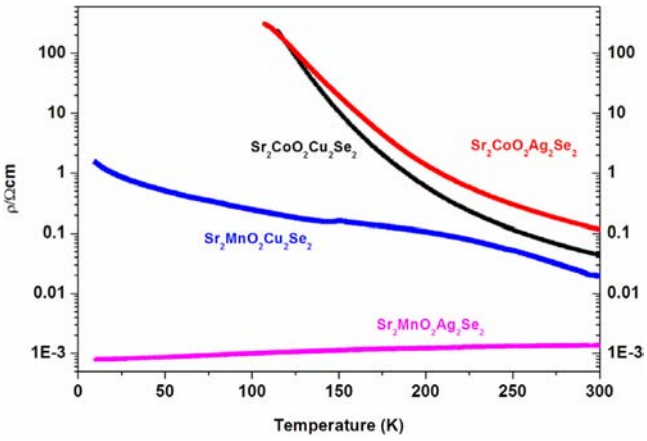

Figure 7. Electrical resistivity as a function of temperature for the samples of $Sr_2CoO_2Cu_2Se_2$ (black), $Sr_2CoO_2Ag_2Se_2$ (red), $Sr_2MnO_2Cu_{1.5}Se_2$ (blue), and $Sr_2MnO_2Ag_{1.5}Se_2$ (pink).

$Sr_2MnO_2Cu_{1.5}S_2$ (~27 Ωcm at 300 K), implying the charge-carrying selenide layers have higher conductivity than the sulfide layers. The resistivity of $Sr_2MnO_2Cu_{1.5}Se_2$ shows an anomalous change in the gradient at 150 K, presumably associated with the structural changes. While for the Co compounds, the resistivity shows less dramatic changes in gradient and can be fitted well to the Steinhart–Hart equation (Figure S1). Surprisingly, the transport properties of the multiphase sample $Sr_2MnO_2Ag_{1.5}Se_2$ turn out to be metallic. The unusual result is probably due to the presence of minor conducing impurities (1.55 mass % Ag) that coexist with the $Sr_2MnO_2Ag_{1.5}Se_2$ sample.

It is well-established that the chalcogenide layers present in the oxysulfides can readily accept holes in the antibonding states at the top of a valence band, and these holes are very mobile. The room temperature Hall effect measurement indicates the conduction of the three phase pure oxyselenides are p-type, and the measured hole mobility for compounds $Sr_2CoO_2Cu_2Se_2$, $Sr_2CoO_2Ag_2Se_2$, and $Sr_2MnO_2Cu_{1.5}Se_2$ are 33.3 $cm^2\ V^{-1}\ S^{-1}$, 69.4 $cm^2\ V^{-1}\ S^{-1}$, and 4.88 $cm^2\ V^{-1}\ S^{-1}$, respectively. The mobilities of those oxyselenides are generally larger than some reported oxysulfides (e.g., 10 $cm^2\ V^{-1}\ s^{-1}$ for bulk LaOCuS).[11] As a general rule, the mobility of those oxychalcogenides tend to increase as the electronegativity of the chalcogen decreases (e.g., 80 $cm^2\ V^{-1}\ s^{-1}$ for bulk LaOCuTe).[11]

Optical Band Gaps. As shown in the inlet of Figure 8, the UV–vis-IR optical measurements (240–2600 nm) were performed on samples $Sr_2CoO_2Cu_2Se_2$, $Sr_2CoO_2Ag_2Se_2$, and $Sr_2MnO_2Cu_{1.5}Se_2$, respectively, with no visible absorption edge being detected between 0.5 and 5.0 eV. A minor drop of absorbance is found for $Sr_2MnO_2Cu_{1.5}Se_2$ between 1.0 eV–1.7 eV, which is presumably arising from intraband transitions. The measurements suggest that the optical band gaps of the three compounds are less than 0.5 eV, consistent with the samples' black color. Figure 8 shows the middle infrared optical absorption spectra (0.05–0.5 eV) of the three compounds, which represent some sharp drops between 0.05 and 0.2 eV, corresponding to the fundamental absorption edges. Beside the absorption edges, the spectra also present several absorption peaks that arise from lattice vibration, some of which are clearer below the absorption edge. The band gap can be estimated to be at the crossover of the absorption edge and the lattice

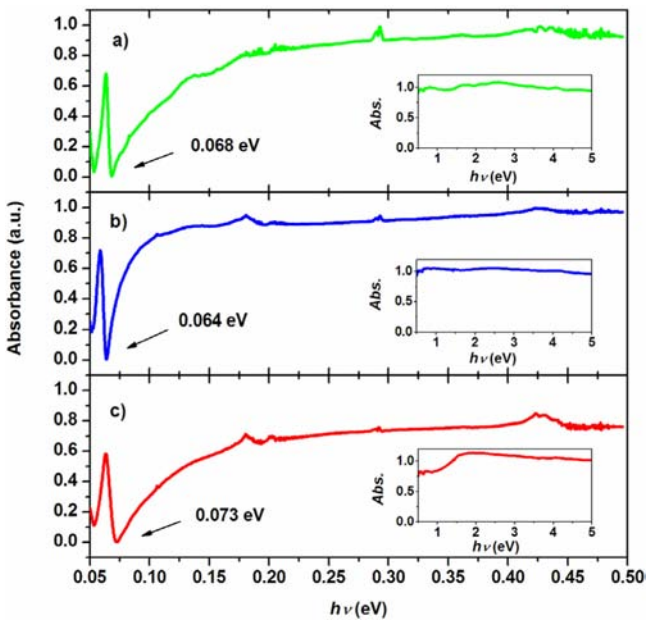

Figure 8. UV–vis-IR absorption spectra (inset) and middle IR absorbance spectra for the samples of $Sr_2CoO_2Cu_2Se_2$ (a), $Sr_2CoO_2Ag_2Se_2$ (b), and $Sr_2MnO_2Cu_{1.5}Se_2$ (c), the band gap is estimated at the crossover of the absorption edge and the lattice vibration peak.

vibration peak. The optical band gaps of $Sr_2CoO_2Cu_2Se_2$, $Sr_2CoO_2Ag_2Se_2$, and $Sr_2MnO_2Cu_{1.5}Se_2$ are then determined to be 0.068, 0.064, and 0.073 eV, respectively. The narrow bandgap of the title compounds are very different from some early reported quaternary oxyselenides, where the typical bandgaps are around 2–3 eV.[11] Moreover, the absorption edge of $Sr_2CoO_2Ag_2Se_2$ is more confined in comparision with the other two copper selenium oxychalcogenides. Further electronic structure calculations may shed light on the behavior of those compounds.

■ CONCLUSIONS

In this work, we extended the range of available $Sr_2Mn_3Sb_2O_2$ type oxychalcogenides to include four new layered oxy-selenides, which contain well-defined distinct metal oxide and metal selenide layers according to the chemical preferences of the metals. The rigid oxide layers of these compounds constrain the basal lattice parameters and result in largely deformed than ideal tetrahedral sites for the copper and silver ions. Specifically, $Sr_2CoO_2Ag_2Se_2$ contains the largest CoO_2 square plane that can be stabilized. The variable occupancy of the metal ion (Cu^+ or Ag^+) in the tetrahedral sites within the selenide layer is determined by oxidizability of the metal oxide layers. Although substitution in the chalcogenide layer did not substantially change the magnetic properties of those oxychalcogenide, they do alter the antiferromagnetic transition temperatures. More than that, transport measurement indicates the p-type conductivity of those oxyselenides is systematically several orders higher than their oxysulfide analogues. Meanwhile, the optical bandgap of those compounds is significantly narrowed to around 0.07 eV. Electronic structure calculations may shed light on those behaviors of this system. The correlation of the low-temperature structures and the magnetic and electronic properties of these phases also invite further detailed investigations.

dx.doi.org/10.1021/ic301022g | Inorg. Chem. 2012, 51, 10185–10192

■ ASSOCIATED CONTENT

Supporting Information

Crystallographic data in CIF format for $Sr_2CoO_2Cu_2Se_2$, $Sr_2CoO_2Ag_2Se_2$, $Sr_2MnO_2Cu_{1.5}Se_2$, and $Sr_2MnO_2Ag_{1.5}Se_2$, results of fitting to temperature dependent resistivity data. This material is available free of charge via the Internet at http://pubs.acs.org.

■ AUTHOR INFORMATION

Corresponding Author

*E-mail: chenx29@iphy.ac.cn.

Notes

The authors declare no competing financial interest.

■ ACKNOWLEDGMENTS

The present work is supported by the National Science Foundation of China (Nos. 90922037 and 51072226). The authors would like to thank Prof. G. Wang, Ms. Y. P. Xu, T. T. Zhou, X. F. Lai, H. Zhang, and Mr. T. P. Ying for very useful discussions.

■ REFERENCES

(1) Vajenine, G. V.; Hoffmann, R. *Inorg. Chem.* **1996**, *35*, 451.
(2) Zhu, W. J.; Hor, P. H.; Jacobson, A. J.; Crisci, G.; Albright, T. A.; Wang, S. H.; Vogt, T. *J. Am. Chem. Soc.* **1997**, *119*, 12398.
(3) Rutt, O. J.; Williams, G. R.; Clarke, S. J. *Chem. Commun.* **2006**, 2869.
(4) Gál, Z. A.; Rutt, O. J.; Smura, C. F.; Overton, T. P.; Barrier, N.; Clarke, S. J.; Hadermann, J. *J. Am. Chem. Soc.* **2006**, *128*, 8530.
(5) Meignen, V.; Cario, L.; Lafond, A.; Moëlo, Y.; Guillot-Deudon, C.; Meerschaut, A. *J. Solid State Chem.* **2004**, *177*, 2810−2817.
(6) Rutt, O. J. D. Phil. Thesis, University of Oxford, Oxford, U.K., 2008.
(7) Palazzi, M.; Carcaly, C.; Flahaut, J. *J. Solid State Chem.* **1980**, *35*, 150−155.
(8) Palazzi, M. *C. R. Seances Acad. Sci., Ser. 2* **1981**, *292*, 7899.
(9) Chan, G. H.; Deng, B.; Bertoni, M.; Ireland, J. R.; Hersam, M. C.; Mason, T. O.; Van Duyne, R. P.; Ibers, J. A. *Inorg. Chem.* **2006**, *45*, 8264.
(10) Hiramatsu, H.; Yanagi, H.; Kamiya, T.; Ueda, K.; Hirano, M.; Hosono, H. *Chem. Mater.* **2008**, *20*, 326−334.
(11) Clarke, S. J.; Adamson, P.; Herkelrath, S. J. C.; Rutt, O. J.; Parker, D. R.; Pitcher, M. J.; Smura, C. F. *Inorg. Chem.* **2008**, *47*, 8473−8486.
(12) Otzschi, K.; Ogino, H.; Shimoyama, J.; Kishio, K. *J. Low Temp. Phys.* **1999**, *117*, 729.
(13) Brechtel, E.; Cordier, G.; Schaefer, H. *Z. Naturforsch., B: Anorg. Chem., Org. Chem.* **1979**, *34*, 777.
(14) Zhu, W. J.; Hor, P. H. *J. Solid State Chem.* **1997**, *130*, 319.
(15) Ueda, K.; Hirose, S.; Kawazoe, H.; Hosono, H. *Chem. Mater.* **2001**, *13*, 1880.
(16) Hirose, H.; Ueda, K.; Kawazoe, H.; Hosono, H. *Chem. Mater.* **2002**, *14*, 1037.
(17) Smura, C. F.; Parker, D. R.; Zbiri, M.; Johnson, M. R.; Gal, Z. A.; Clarke, S. J. *J. Am. Chem. Soc.* **2011**, *133*, 2691.
(18) Herkelrath, S. J. C.; Saratovsky, I.; Haderman, J.; Clarke, S. J. *J. Am. Chem. Soc.* **2008**, *130*, 14426−14427.
(19) Boultif, A.; Louër, D. *J. Appl. Crystallogr.* **1991**, *24*, 987−993.
(20) Rodríguez-Carvajal. *Satellite Meeting on Powder Diffraction of the XV Congress of the IUCr*, Toulouse, France, 1990.
(21) Cario, L.; Lafond, A.; Morvan, T.; Kabbour, H.; André, G.; Palvadeau, P. *Solid State Sci.* **2005**, *7*, 936.
(22) Barrier, N.; Clarke, S. J. *Chem. Commun.* **2003**, *1*, 164−165.
(23) Oku, M.; Hirokawa, K.; Ikeda, S. *J. Electron Spectrosc. Relat. Phenom.* **1975**, *7*, 465−473.
(24) Tauc, J. *Mater. Res. Bull.* **1968**, *3*, 37.